








Widely Tunable III–V/Silicon Lasers for Spectroscopy in the Short-Wave Infrared

Ruijun Wang , Bahawal Haq, Stephan Sprengel, Aditya Malik , Anton Vasiliev , Gerhard Boehm, Ieva Šimonytė, Augustinas Vizbaras , Kristijonas Vizbaras, Joris Van Campenhout , Roel Baets , Markus-Christian Amann, and Gunther Roelkens 

(Invited Paper)

Abstract—Integrating III–V gain material with silicon photonic integrated circuits enables the realization of advanced laser sources and full integrated systems for optical communication and sensing applications. The availability of III–V/silicon laser sources operating in the 2–2.5 μm short-wave infrared wavelength range is very valuable for spectroscopic sensing since many important industrial gases and blood glucose have absorption bands in this wavelength range. In this paper, first we present our latest results on heterogeneously integrated III–V-on-silicon distributed feedback (DFB) laser arrays. A III–V-on-silicon DFB laser array covering the 2.27–2.39 μm wavelength range with 6 nm wavelength spacing is reported. This DFB laser array is employed as the light source for tunable diode laser absorption spectroscopy of different gases. A four-channel DFB laser array integrated with a beam combiner is used to perform spectroscopic sensing over a 7 nm spectral range without mode hopping at room temperature. Finally, we present our recent advances in widely tunable Vernier lasers based on heterogeneous integration and butt-coupling of the gain section. Continuous tuning near the absorption lines by thermally adjusting the laser cavity length enables high-resolution tunable diode laser absorption spectroscopy measurements together with wide wavelength coverage.

Index Terms—Semiconductor lasers, laser array, laser tuning, silicon photonics, mid-infrared.

I. INTRODUCTION

THE development of silicon photonics in recent years has enabled low-cost and high-speed integrated optical transceivers used in short-distance data communication and long-haul optical transmission [1]. Integrating III–V materials or prefabricated III–V gain chips with silicon photonic integrated circuits (ICs) provides a practical solution to implement laser sources for silicon photonics applications [2]–[5]. This III–V/silicon hybrid approach also can be used to make advanced laser sources for optical communication and sensing applications since the silicon photonics platform can provide ultra-compact and high-performance photonic components, such as low-loss spiral waveguides, high-Q micro-ring resonators (MRRs) [6], low-loss on-chip beam combiners [7], and widely tunable filters [8]. For example, Z. Wang *et al.* demonstrated a passively mode-locked laser operating at 1.6 μm wavelength with a record-low repetition rate of 1 GHz by heterogeneously integrating a III–V-on-silicon semiconductor optical amplifier (SOA) with a 3.7 cm long silicon-on-insulator (SOI) spiral waveguide (propagation loss ~ 0.7 dB/cm) [9]. T. Kita *et al.* realized a III–V/silicon hybrid laser with a very wide wavelength tuning range that can cover the C-band (1530–1565 nm) and L-band (1565–1625 nm) of the optical communications window by using two silicon MRRs and an asymmetric Mach-Zehnder interferometer as the wavelength tuning filter [10]. Besides, the integration of III–V/silicon lasers with silicon photonic ICs enables fully integrated spectroscopic sensors for applications such as gas sensing [11] and bio-sensing [12]. In order to realize on-chip silicon photonic spectroscopic sensors, many efforts have been devoted to develop silicon waveguide-based components to probe the analyte [13]–[15]. However, in these on-chip silicon photonic sensors, the light from an external laser source is coupled to the chip for the absorption spectroscopy measurement, instead of using an integrated light source [11]–[15]. In order to realize a compact spectroscopic sensor, a chip-scale laser source should be integrated with the probe components. Therefore, realizing a III–V/silicon laser source is also a critical step towards on-chip silicon photonic spectroscopic sensors.

Manuscript received February 6, 2019; revised June 12, 2019; accepted June 12, 2019. Date of publication June 24, 2019; date of current version August 13, 2019. This work was supported in part by Grant FP7-ERC-PoC-FireSpec and in part by the INTERREG Safeside Project. (Corresponding author: Ruijun Wang.)

R. Wang was with the Photonics Research Group, Center for Nano- and Biophotonics, Ghent University-IMEC, B-9052 Ghent, Belgium. He is now with the Institute for Quantum Electronics, 8000-8099 Zürich, Switzerland (e-mail: ruiwang@phys.ethz.ch).

B. Haq, A. Vasiliev, R. Baets, and G. Roelkens are with the Photonics Research Group, Center for Nano- and Biophotonics, Ghent University-IMEC, B-9052 Ghent, Belgium (e-mail: bahawal.haq@ugent.be; anton.vasiliev@ugent.be; Roel.Baets@UGent.be; Gunther.Roelkens@UGent.be).

S. Sprengel, G. Boehm, and M.-C. Amann are with the Walter Schottky Institut, Technischen Universität München, 85748 Garching, Germany (e-mail: stephan.sprengel@wsi.tum.de; Gerhard.Boehm@wsi.tum.de; mcamann@wsi.tum.de).

A. Malik was with the Photonics Research Group, Center for Nano- and Biophotonics, Ghent University-IMEC, B-9052 Ghent, Belgium. He is now with the Department of Electrical and Computer Engineering, University of California Santa Barbara, Santa Barbara, CA 93106 USA (e-mail: amalik@ece.ucsb.edu).

I. Šimonytė, A. Vizbaras, and K. Vizbaras are with the Brolis Semiconductors UAB, LT-14259 Vilnius, Lithuania (e-mail: ieva.simonyte@brolis-semicon.com; augustinas.vizbaras@brolis-semicon.com; kristijonas.vizbaras@brolis-semicon.com).

J. Van Campenhout is with the IMEC, 3001 Leuven, Belgium (e-mail: joris.vancampenhout@imec.be).

Color versions of one or more of the figures in this paper are available online at <http://ieeexplore.ieee.org>.

Digital Object Identifier 10.1109/JSTQE.2019.2924109

Tunable semiconductor lasers operating in the 2–2.5 μm wavelength range are very relevant for trace gas sensing since many important industrial gases (e.g., CO_2 , CO , CH_4 , NH_3 , C_2H_2) have strong absorption lines in this spectral region [16]. Compared with the near infrared region, the stronger absorption cross section of the molecules enable optical gas sensors to operate in this wavelength range with higher sensitivity. Although the mid-infrared spectral region ($>2.5 \mu\text{m}$) offers even stronger absorption, in the 2–2.5 μm wavelength range the cheaper photonic components and low-noise photodetectors enable low-cost and miniaturized optical sensors without e.g., an extra cooling system. Among different semiconductor lasers, InP-based and GaSb-based distributed feedback (DFB) lasers and vertical cavity surface emitting lasers (VCSELs) have shown very good performance in the 2–2.5 μm wavelength range [17]–[20]. However, the tuning range of a single DFB laser and VCSEL is limited around 3–5 nm. The development of widely tunable InP-based and GaSb laser sources operating in this spectral region would allow to simultaneously detect different gases. It is also very valuable for bio-sensing considering the broad absorption features of bio-molecules. For example, blood glucose has a strong combination absorption band in the 2–2.3 μm wavelength range [21]. In this wavelength range, GaSb-based gain chips coupled to a diffraction grating used for wavelength selection have shown wide tunability [22]. However, the bulky optic system and mechanical controller used in these widely tunable lasers make it less suitable for portable, low-cost optical sensing.

For the 2–2.5 μm wavelength range, semiconductor lasers based on InP-based type-I, type-II and GaSb-based type-I heterostructures have shown high performance [17]–[20]. Among these material systems, laser diodes based on the GaSb-based type-I quantum wells exhibit the best performance and can lase above 3 μm wavelength [23]. However, the heterogeneous integration processes of GaSb-based materials are not as well-established as for InP-based materials, which results in a low process yield and poor device performance so far [24]. Heterogeneously integrated InP-type-I Fabry-Perot lasers on silicon operating at 2.0 μm wavelength have been demonstrated [25]. However, the emission wavelength of InP-based type-I quantum well lasers is limited to around 2.3 μm [26]. In recent years, InP-based type-II quantum well laser diodes with emission wavelength up to 2.7 μm wavelength have been realized by employing “W”-shaped InGaAs/GaAsSb quantum wells as the active region [27]. In this paper, we present three different types of chip-scale widely tunable lasers based on the heterogeneous integration of InP-based type-II materials on silicon or by butt-coupling a prefabricated GaSb gain chip with silicon photonic ICs. The paper is organized as follows. Section II introduces the heterogeneous integration process of InP-based type-II materials and the design of the optical coupling between the III–V waveguide and silicon waveguide. Section III discusses our recent results on InP-based type-II DFB laser arrays on silicon and their application in gas sensing. Section IV focuses on heterogeneously integrated widely tunable Vernier lasers, while Section V is devoted to the widely tunable GaSb/silicon external cavity laser. Finally, the paper is concluded in Section VI.

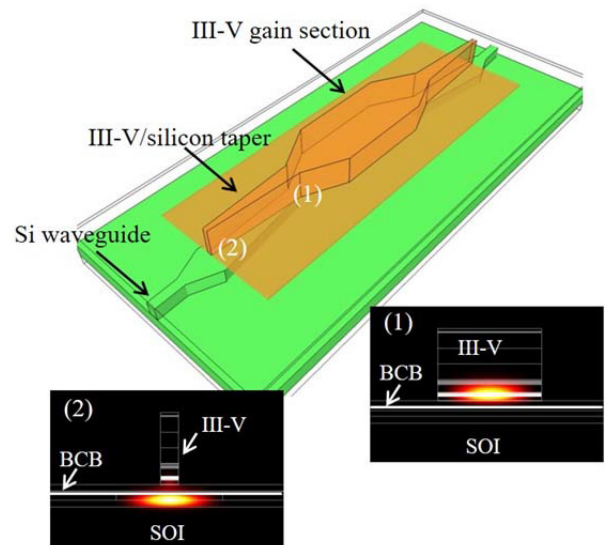


Fig. 1. Schematic of the III-V-on-silicon semiconductor optical amplifier. The mode intensity distribution in the III-V/silicon hybrid waveguide at two positions is shown as an inset.

II. HETEROGENEOUSLY INTEGRATED III-V-ON-SILICON LASERS

A heterogeneously integrated InP-based type-II quantum well laser consists of a III-V-on-silicon semiconductor optical amplifier (SOA) and silicon waveguide-based feedback circuit. Fig. 1 shows the schematic of the III-V-on-silicon SOA. The SOA is adhesively bonded on a silicon rib waveguide with an etch depth of 180 nm in a 400 nm silicon device layer and consists of a gain section in the center and two III–V/silicon spot size converters (SSCs) on both sides. In the gain section, the optical mode is strongly confined in the III–V waveguide to ensure a high modal gain. The III–V epitaxial layer stack consists of a 200 nm thick n -InP contact layer, an active region sandwiched between a 130 nm thick GaAsSb and a 250 nm thick AlGaAsSb separate confinement heterostructure layer, a 1.5 μm thick p -InP cladding layer and a 100 nm thick p -InGaAs contact layer. The active region contains six periods of a “W”-shaped quantum well structure, each separated by a 9 nm tensile strained GaAs_{0.58}Sb_{0.42} layer. Every quantum well structure consists of a 2.9 nm thick GaAs_{0.33}Sb_{0.67} layer surrounded by two 2.6 nm thick In_{0.68}Ga_{0.32}As layers. The calculated confinement factor of the TE polarized fundamental mode in the quantum wells is around 10%. An efficient light coupling between the silicon waveguide and III–V waveguide is achieved by the III–V/silicon SSCs. The SSCs have two tapered section as shown in Fig. 1. In the first section, the III–V waveguide is linearly tapered from 5 μm to 1.2 μm over a length of 50 μm . In the second section, the III–V waveguide is linearly tapered to a very narrow tip where the silicon waveguide is tapered from 0.2 μm to 3 μm . The second section is an adiabatic inverted taper coupler, where the optical mode is gradually transferred from the III–V waveguide to silicon waveguide (and vice versa) as shown in Fig. 1. The simulated coupling efficiency of the III–V/silicon SSC is around 90% when the III–V taper tip is 0.5 μm wide. Detailed information on the design of

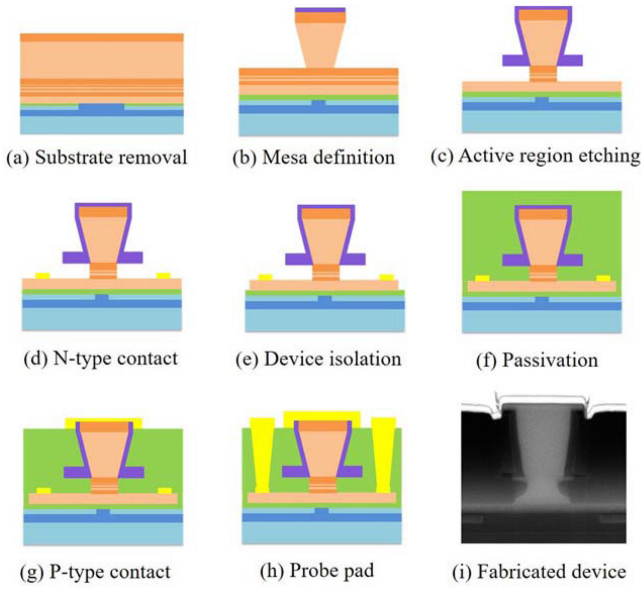


Fig. 2. Process flow for the fabrication of III-V-on-silicon lasers.

the III-V/silicon SSC can be found in Ref. [28]. The fabrication process of heterogeneously integrated InP-based type-II quantum well lasers can be divided into two parts: firstly the silicon waveguide circuits are processed in a CMOS pilot line on 200 mm SOI wafers, then the laser sources are fabricated in a III-V-on-silicon device platform developed for optical communication and sensing applications. In the CMOS pilot line, the waveguides are etched 180 nm deep in the 400 nm thick silicon device layer. To achieve a high-yield and uniform bonding, the silicon wafer is planarized by SiO₂ deposition followed by a chemical mechanical polishing down to the silicon device layer. Then the III-V epitaxial layer is adhesively bonded to the silicon waveguide circuits by a 50 nm thick divinylsiloxane-bis-benzocyclobutene (DVS-BCB) bonding layer. The absorption coefficient of DVS-BCB is around 10 cm⁻¹ in the 2–3 μm wavelength range [29]. The following process steps are shown in Fig. 2. After bonding, the InP substrate is removed using HCl wet etching (Fig. 2(a)). Then the integrated lasers are processed on the III-V-on-silicon membrane. Firstly, a 200 nm SiN_x layer is deposited on the sample as a hard mask. Then the III-V waveguide is defined using 320 nm UV contact lithography. After dry etching of the SiN_x hard mask and the *p*-InGaAs contact layer, the 1.5 μm thick *p*-InP cladding layer is etched using a 1:1 HCl:H₂O solution (Fig. 2(b)). This anisotropic wet etching creates a “V”-shaped undercut, which ensures the III-V/silicon SSC have a very narrow taper tip, leading to an efficient coupling between the III-V waveguide and silicon waveguide. Afterwards, a second SiN_x hard mask is deposited on the sample to protect the III-V taper tip in the following wet etching. Then the active region is etched in a 1:1:20:70 H₃PO₄:H₂O₂:Citric Acid:H₂O solution using the *n*-InP layer as the etch stop layer (Fig. 2(c)). Afterwards, Ni/Ge/Au is deposited on the *n*-InP layer (Fig. 2(d)). After metallization and lift-off, the *n*-InP is etched by 1:1 HCl:H₂O to isolate different devices (Fig. 2(e)). Then a ~3.5 μm thick DVS-BCB layer is spin-coated on the sample

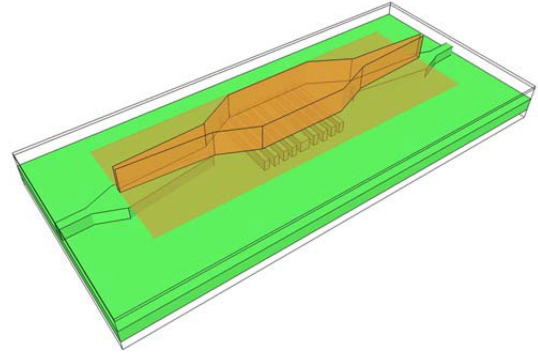


Fig. 3. Schematic of the heterogeneously integrated III-V-on-silicon DFB laser.

to passivate the devices (Fig. 2(f)). After curing, the DVS-BCB layer is etched back to the *p*-InGaAs layer to expose this contact layer. Subsequently, Ti/Au is deposited on the sample as *p*-contact (Fig. 2(g)) and probe pad (Fig. 2(h)). A scanning electron microscope (SEM) image of the fabricated III-V-on-silicon lasers is shown in Fig. 2(i). This fabrication process is the same as that of the III-V-on-silicon photodetectors operating in the 2–2.5 μm wavelength range [30], thereby fully integrated spectroscopic sensors can be realized based on a single epitaxial layer stack and process flow.

III. HETEROGENEOUSLY INTEGRATED 2.3 μm III-V-ON-SILICON DFB LASER ARRAY

A. Single III-V-on-Silicon DFB Laser

In a heterogeneously integrated InP-based type-II DFB laser a first-order DFB grating is implemented underneath the III-V-on-silicon SOA as schematically shown in Fig. 3. In the device, the tail of the optical mode interacts with the DFB grating, which selects the emission wavelength of the laser. In order to have stable single mode lasing, a quarter-wave shifted grating structure is used to break the modal degeneracy. The coupling coefficient κ of this DFB grating is calculated to be 80 cm⁻¹. Since the gain section length of the DFB lasers shown in this paper is 700 μm, the normalized coupling coefficient κL of these DFB lasers is around 5.6. The integrated lasers are mounted on a temperature-controlled stage during measurements. The light in the silicon waveguide is coupled to a standard single-mode fiber (SMF-28) via integrated chip-to-fiber couplers. To determine the waveguide-couple optical output power of the DFB laser, the fiber-to-chip coupler loss is measured on reference structures on the same wafer. An optical spectrum analyzer (OSA, Yokogawa AQ6375) is used to study the optical output power and emission spectra of the lasers. Fig. 4 shows the continuous wave (CW) on-chip output power-current (L-I) curve of a heterogeneously integrated InP-based type-II DFB laser with a silicon DFB grating pitch of 347 nm. In CW regime, the laser can operate till about 25 °C. The maximum on-chip output is 1.3 mW at 5 °C and reduces to 0.38 mW at 20 °C, while the threshold current increases from 52 mA to 76 mA. The performance of this III-V-on-silicon laser is comparable to state-of-the-art InP-based type-II quantum well lasers on InP substrate [27], [31]. Further improvement

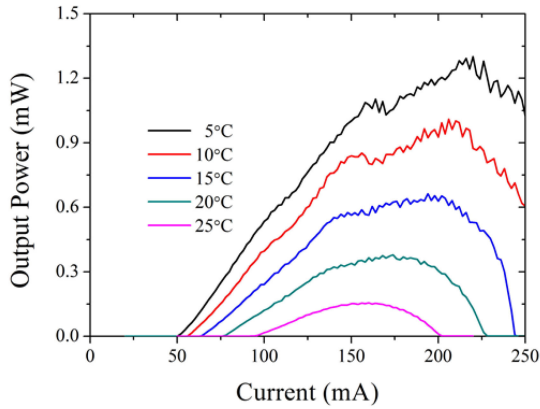


Fig. 4. CW light-current (L-I) curve of the III-V-on-silicon DFB laser with grating pitch of 347 nm.

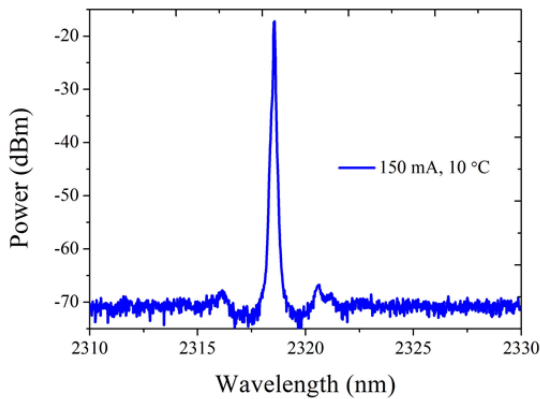


Fig. 5. Fiber-coupled laser spectrum of the III-V-on-silicon laser with DFB grating pitch of 347 nm.

can be realized by optimizing the III–V epitaxial layer stack, especially the current injection efficiency [27], e.g., introducing additional gradings at the heterobarriers between n-InP and n-GaAsSb. A fiber-coupled lasing spectrum of the device for a bias current 150 mA at 10 °C is shown in Fig. 5. The dominant mode is located at 2318.5 nm. Single mode emission with a side mode suppression ratio (SMSR) of 50 dB is achieved.

High-performance tunable diode laser absorption spectroscopy (TDLAS) requires laser sources with stable and mode-hop-free tuning. The spectral map of the DFB laser with 347 nm grating pitch as a function of the bias current at 5 °C and 20 °C is shown in Fig. 6. In both maps, the emission spectra are single mode with a very high SMSR of more than 40 dB throughout the current range. The lasing wavelength linearly changes with the bias current. The device exhibits more than 4 nm and 2.5 nm mode-hop-free tuning at 5 °C and 20 °C, respectively. The current-tuning coefficient is around 0.02 nm/mA at 5 °C and 0.018 nm/mA 20 °C. A single DFB laser has more than 6 nm current-tuning range when varying the chip temperature between 5 °C to 25 °C. Therefore, a broad wavelength coverage III-V-on-silicon DFB laser array with wavelength spacing around 6 nm can be used to detect any absorption features of molecules in this spectral range. Compared with our previously demonstrated heterogeneously integrated InP-based type-II DFB laser [32], [33],

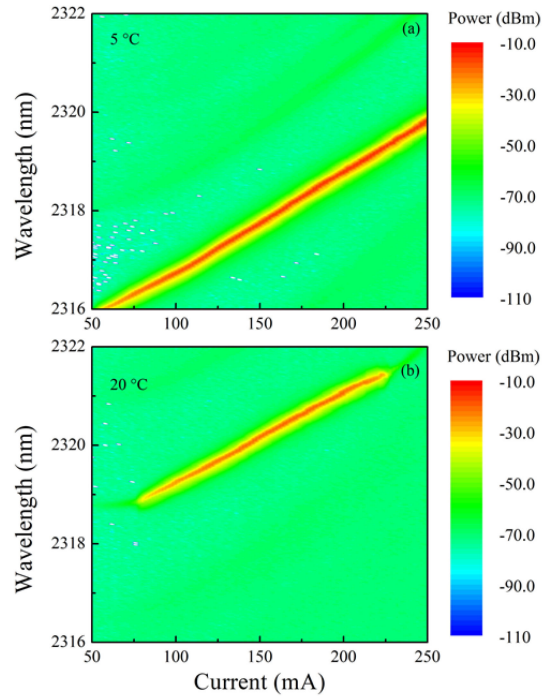


Fig. 6. Spectral map of fiber-coupled emission from the III-V-on-silicon DFB laser with grating pitch of 347 nm at 5 °C and 20 °C.

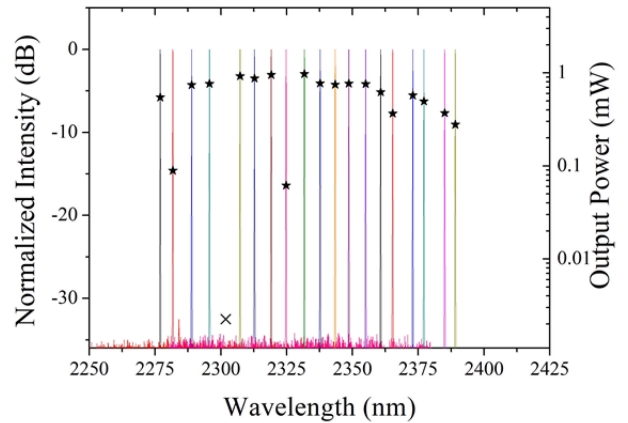


Fig. 7. Normalized emission spectra and output power (indicated by the stars) of III-V-on-silicon DFB lasers with a silicon grating pitch ranging from 340 nm to 359 nm.

the device shown here can operate in CW at room temperature and above without mode-hopping.

B. III–V-on-Silicon DFB Laser Array

We have demonstrated III-V-on-silicon DFB laser arrays with wavelength spacing of 30 nm at 2.35 μm wavelength range [33]. In order to achieve complete spectral coverage, in this paper we report a heterogeneously integrated InP-based type-II DFB laser array with a wavelength spacing of 6 nm (combined with the wavelength tuning discussed above). Here we take advantage of the state-of-the-art silicon photonics pilot line to fabricate silicon grating arrays with a pitch increment of 1 nm. Fig. 7 shows the normalized lasing spectra of a III-V-on-silicon DFB laser array

with grating pitch variation of 1 nm. Most of the lasers are measured at 10 °C while the lasers with grating pitch of 341 nm and 355 nm are measured at 5 °C since these two lasers stop lasing at 10 °C. All lasers are operated CW regime with a bias current of 180 mA. It can be found that a SMSR higher than 30 dB can be achieved for all of lasers. The emission wavelength shifts from 2277 nm to 2289 nm as the DFB grating pitch increases from 340 nm to 359 nm. 1 nm change in the grating pitch results in 6 nm change in the emission wavelength. The laser with a grating pitch of 344 nm did not lase because of material defects in the III–V waveguide, which could be observed during device processing. The output power of some lasers is substantially lower than others since these lasers have epitaxial material defects located in the III–V taper, which introduce a large loss in the III–V/silicon SSC. The wavelength coverage of this DFB laser array overlaps with absorption bands of many gases, e.g., CO, CH₄, NH₃, HF, C₂H₂. Therefore, it can be used to detect these gases from absorption lines within this spectral range.

The heterogeneously integrated III-V-on-silicon DFB laser array was then used to detect NH₃ and CO based on direct absorption spectroscopy. In the NH₃ sensing setup, the light is coupled from the III-V-on-silicon chip to a single-mode fiber through the integrated on-chip grating coupler, and then coupled to a NH₃ gas cell. The 5.5 cm-long fiber-coupled gas cell contains pure NH₃. DFB lasers with a grating pitch of 343 nm and 347 nm are used to detect NH₃ since their wavelength tuning range overlaps with two strong absorption lines of NH₃. During measurements, the DFB laser with grating pitch of 343 nm is operated at a heat-sink temperature of 20 °C, while the 347 nm device is operated at 15 °C. As the bias current increases, the lasing wavelength is tuned and scanned over the absorption lines of NH₃, showing a dip in the L-I curve. Based on the pre-measured current-wavelength relationship, the absorption spectra can be reconstructed. In these NH₃ spectroscopic measurements, both DFB lasers are tuned in a current step of 2 mA, which corresponds to a wavelength step of around 36 pm. The measured absorption spectra of NH₃ and the corresponding high-resolution transmission molecular absorption (HITRAN) spectra are shown in Fig. 8(a) and 8(b). Good agreement can be observed. In the CO sensing setup, the light from the III-V-on-silicon chip is coupled to a free space gas cell through a collimator. The 10 cm-long CO gas cell contains pure CO and is AR-coated for a wavelength range around 2.35 μm. The DFB laser with grating pitch of 352 nm operated at 10 °C and that with a pitch of 358 nm operated at 5 °C are used. Since CO has much narrower absorption lines than NH₃, the DFB lasers are tuned with a current step of 0.2 mA in the CO sensing measurements, which corresponds to a wavelength step of 4 pm. From the measurement results shown in Fig. 9(a) and 9(b) and its comparison with the HITRAN data, one can conclude that the III-V-on-silicon DFB laser array is also suitable for gases with very narrow absorption features.

C. Combined III–V-on-Silicon DFB Laser Array

For the DFB laser array, the light emitted from different lasers should be combined to a single waveguide for applications in

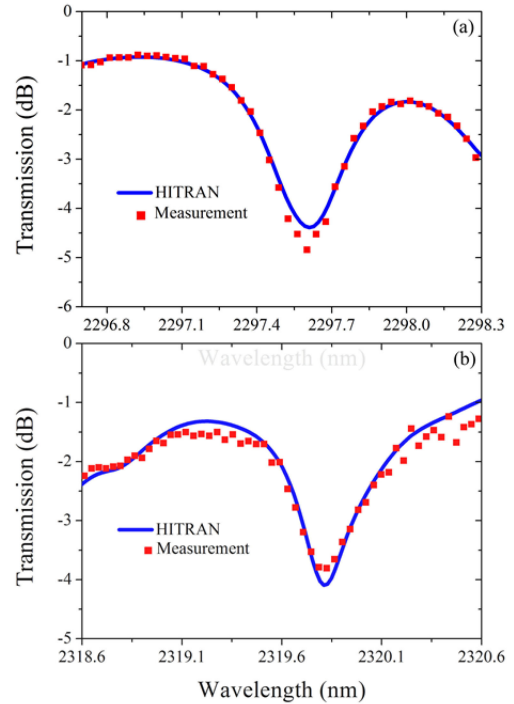


Fig. 8. TDLAS spectra of NH₃ using DFB laser with grating pitch of (a) 343 nm at 20 °C, and (b) 347 nm at 15 °C.

multi-species trace gas spectroscopy [34]. In the telecommunication wavelength range, many types of beam combiners have been developed in integrated optics for wavelength division multiplexing (WDM) optical communications, such as multimode interference (MMI) couplers and funnel combiners [35]. The silicon photonics platform can also provide a low-cost solution to realize high-performance and compact beam combiners for the short-wave infrared wavelength range. In this paper we demonstrate III-V-on-silicon DFB laser arrays integrated with a beam combiner based on cascade 1 × 2 MMI couplers for applications in broadband spectroscopy and multi-species trace gas sensing. Fig. 10(a) shows a microscope image of a four-wavelength DFB laser array integrated with the beam combiner. The DFB laser array has a separation of 120 μm between the different devices, which share a large *p*-contact pad that is also used as a heat spreader. The beam combiner consists of two stages of 1 × 2 MMI couplers and S-bend SOI waveguides as shown in Fig. 10(b). The S-bend waveguides from the DFB laser to the MMI coupler have a bending radius of 50 μm and those between two MMIs has a bending radius of 100 μm. The MMI couplers behave as 50/50 splitter/combiners and were chosen because of their small size and high tolerance to fabrication errors. The 1 × 2 MMI couplers have a length of 28.5 μm and a width of 6.5 μm. A simulated field-intensity distribution of the 1 × 2 MMI coupler when used as a splitter is shown in Fig. 10(c). The insertion loss of the MMI coupler is lower than 0.3 dB in simulation.

Fig. 11(a) shows the normalized emission spectra of a beam combined four-wavelength laser array with different DFB grating pitches. All lasers are biased at 180 mA and operating at 15 °C during measurements. The silicon grating pitch varies

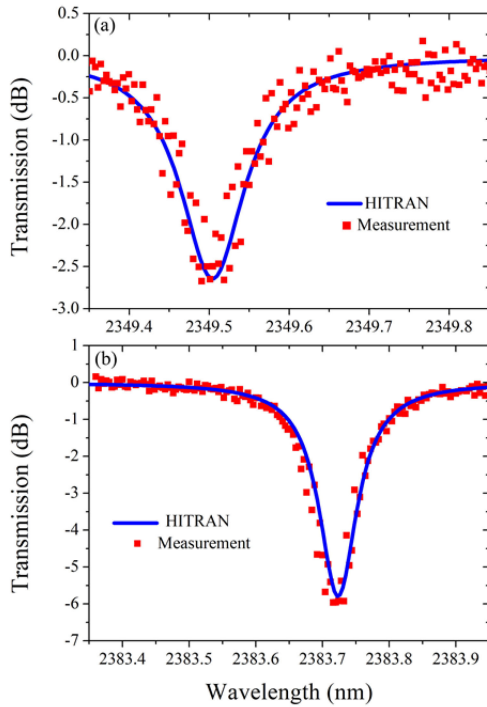


Fig. 9. TDLAS spectra of CO using DFB laser with grating pitch of (a) 352 nm at 10 °C and (b) 358 nm at 5 °C.

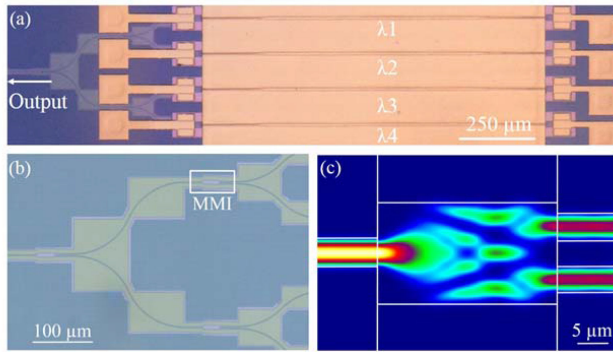


Fig. 10. (a) Microscope image of a four-wavelength III-V-on-silicon DFB laser array integrated with a cascaded MMI beam combiner. (b) Zoom-in on the silicon waveguide-based beam combiner. (c) Simulated intensity distribution as the light propagates through the 1×2 MMI coupler.

from 347 nm to 353 nm with a step of 2 nm. The lasing wavelengths of these lasers are located at 2318.9 nm, 2330.9 nm, 2343 nm and 2355 nm. A wavelength spacing of 12 nm is achieved. Besides varying the silicon grating pitch, the lasing wavelength of DFB lasers also can be controlled by adjusting the width of the III-V waveguide, which enables very small wavelength spacing between different channels. Fig. 11(b) shows four beam combined lasers (with the same grating pitch) with III-V waveguide widths from 3.8 μm to 6 μm when driven at the same condition as the array shown in Fig. 11(a). The wavelength spacing in this laser array is around 1.4 nm. The optical loss in the beam combiners can be extracted by comparing the optical power in the common output waveguide and the waveguide connected with each device on the other side (as the DFB

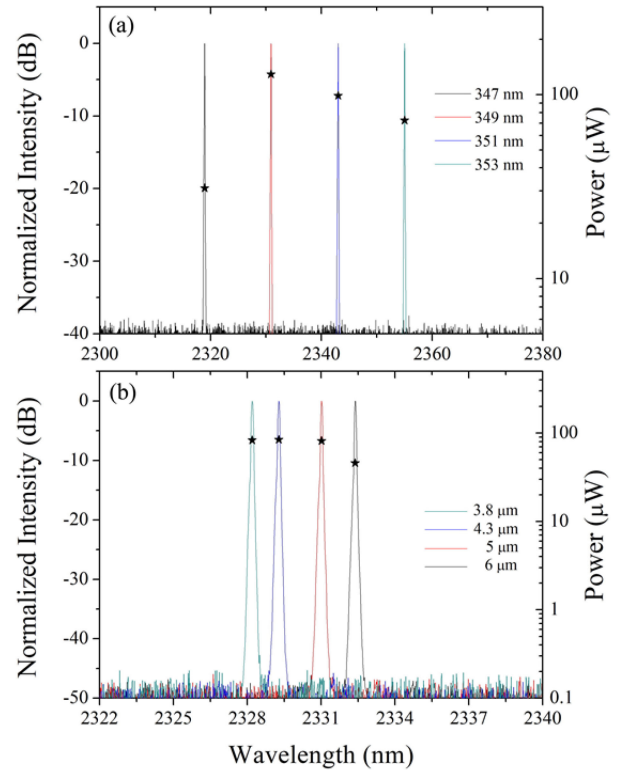


Fig. 11. Normalized emission of the beam combined III-V-on-silicon laser arrays: four DFB lasers with (a) different silicon grating pitches, (b) different III-V waveguide widths. All of lasers in each arrays are measured at the same condition. In both figures, the on-chip peak output powers are indicated by stars.

laser structures are symmetrical). In both III-V-on-silicon DFB laser arrays, the loss is around 6.5–7 dB for every channel. The output powers of these lasers are indicated by stars as shown in Fig. 11. This loss mainly comes from the 3 dB loss in every 1×2 MMI combiner. By heterogeneously integrating a III-V-on-silicon SOA on the output waveguide, this loss can be compensated. For this, we have demonstrated a heterogeneously integrated InP-based type-II SOA with peak gain of ~ 10 dB and 3 dB bandwidth of 150 nm near 2.35 μm wavelength. An alternative solution to reduce the loss in beam combining is replacing the beam combiners with an AWG with low-loss and flat-top passband [36]. Besides, Mach-Zehnder based optical switches also can be used as beam combiners.

The beam combined III-V-on-silicon DFB laser array can be used for a variety of spectroscopic applications. For example, the laser array with large wavelength spacing (e.g., the one shown in Fig. 11(a)) can be used for multi-species trace gas sensing in a broad (>120 nm) spectral range. In this array, each channel can be controlled to lase around a strong absorption line of one gas, that does not overlap with absorption lines of other gases. The laser array with small wavelength spacing can be used for mode-hop free spectroscopy over an extended wavelength range, by only adjusting the bias current of different devices without changing the heat-sink temperature to tune the lasing wavelength. Here we show its application for TDLAS of NH_3 in a >7 nm spectral range as shown in Fig. 12. The beam combined lasers shown in Fig. 10(b) are operated at room

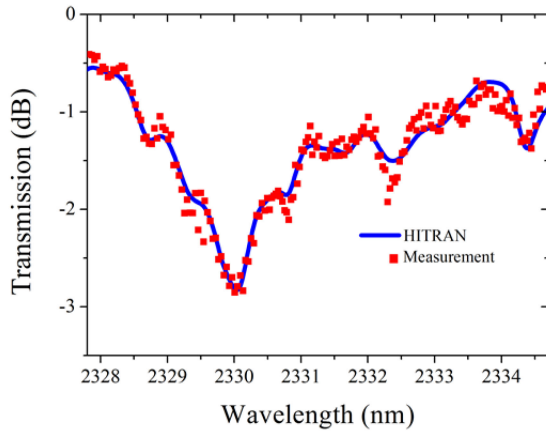


Fig. 12. TDLAS spectrum of NH_3 obtained with the beam combined laser array with different III-V waveguide widths and the corresponding HITRAN spectrum.

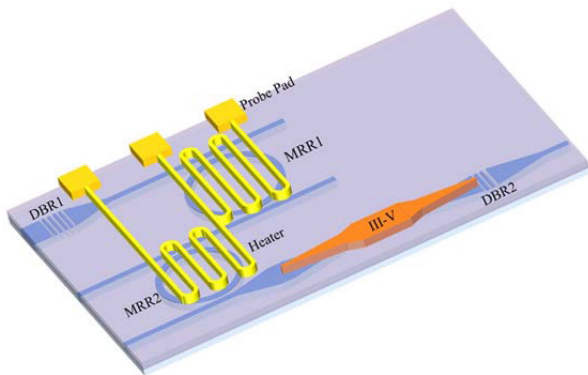


Fig. 13. Schematic of the III-V-on-silicon Vernier laser.

temperature during measurements. The $3.8 \mu\text{m}$ wide DFB laser covers the wavelength range from 2327.8 nm to 2330.2 nm, the $4.3 \mu\text{m}$ one covers 2330.2 nm to 2331.3 nm, the $5 \mu\text{m}$ one covers 2331.3 nm to 2333.1 nm and the $6 \mu\text{m}$ one covers 2333.1 nm to 2335 nm. A good match with the HITRAN data, also shown in Fig. 12, can be observed. These spectroscopic measurement results prove that these III-V-on-silicon DFB laser arrays can be used as the light source for multi-species trace gas sensing and broadband sensing.

IV. WIDELY TUNABLE 2.3 μm III-V-ON-SILICON VERNIER LASER

In the last section, we showed that integrating a series of DFB lasers with silicon photonics beam combiners enables widely tunable single-mode laser sources with mode hop free tuning. In this section, we summarize our recent results on another solution to realize widely tunable laser sources for spectroscopy: heterogeneously integrating short-wave infrared III-V SOAs with widely tunable silicon photonic filters [37]. The schematic of a widely tunable III-V-on-silicon laser using a silicon photonics Vernier filter to select the lasing wavelength is shown in Fig. 13. The Vernier filter and an InP-based type-II quantum well SOA are integrated in a silicon waveguide-based Fabry-Perot laser

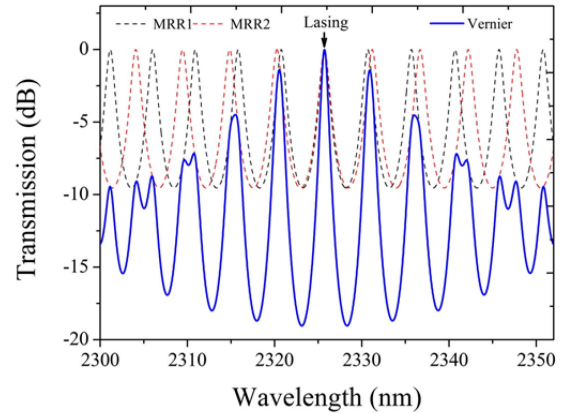


Fig. 14. Simulated transmission spectra of the silicon micro-ring resonators and Vernier filter.

cavity. The epitaxial layer stack design is the same to the one used in the DFB lasers shown in the last section. The Fabry-Perot laser cavity is formed between a high-reflectivity and relatively low-reflectivity silicon DBR (DBR1 and DBR2 respectively). The light is coupled out from the laser cavity to a single mode silicon waveguide through DBR2. The Vernier filter consists of two silicon micro-ring resonators (MRRs) with slightly different radii. The radius of MRR1 and MRR2 is $49.1 \mu\text{m}$ and $44.7 \mu\text{m}$, respectively. The different radii lead to different free spectral ranges (FSRs). The FSR of MRR1 and MRR2 is 5 nm and 5.5 nm, respectively. Fig. 14 shows the calculated transmission spectra of the two MRRs and the corresponding Vernier filter, assuming an MRR quality factor $Q = 2000$ and no waveguide loss. The FSR of the Vernier filter is 55 nm. The transmission of the Vernier filter reaches a maximum when the resonant peaks of the MRRs overlap. Therefore, the lasing wavelength of the III-V-on-silicon Vernier laser is determined by the alignment of the MRR transmission spectra. In order to tune this wavelength position, a microheater is integrated on the MRRs to tune the resonant peak by the thermo-optic effect. The microheaters are patterned and deposited on the DVS-BCB passivation layer after the III-V-on-silicon processes described in Section II.

Fig. 15 shows CW superimposed lasing spectra and output power (indicated by the stars) of a III-V-on-silicon Vernier laser with a DBR pitch of 435 nm and a MRR Q-factor of 5000 at 0°C . A 30 nm wavelength tuning centered at $2.34 \mu\text{m}$ is achieved by varying the electrical power dissipated in the microheater on top of MRR2. In the tuning, 29 mW change in the heater power dissipation leads to a 5 nm change in the lasing wavelength. In this device, the microheaters are deposited on a $1.8 \mu\text{m}$ thick DVS-BCB passivation layer to avoid optical coupling between the silicon waveguide and heater. Because the DVS-BCB is a low thermal conductivity material, the tuning range of the laser is limited by the maximum electrical power that can be dissipated in the microheater and the thermal tuning efficiency. Reducing the DVS-BCB gap between the silicon waveguide and microheater can improve the thermal tuning efficiency and maximum affordable power dissipation. Therefore, we also fabricated III-V-on-silicon lasers with a $1 \mu\text{m}$ DVS-BCB gap. The wavelength

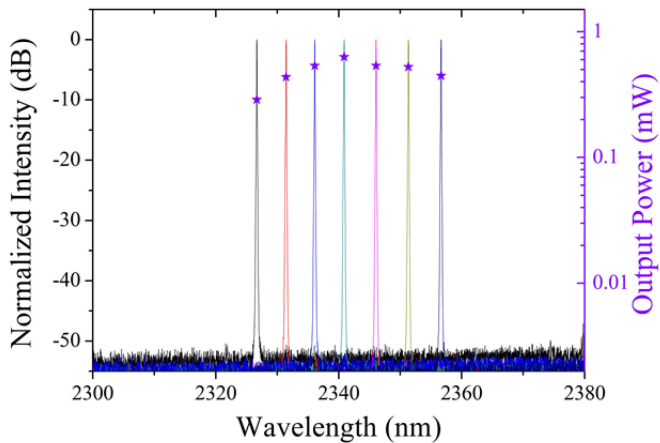


Fig. 15. Superimposed CW laser spectra and output power of the III-V-on-silicon Vernier laser for different power dissipation in the micro-heater on MRR2. The on-chip peak output powers are indicated by stars.

tuning range of this laser is improved to 50 nm at 5 °C (when operated in pulsed mode). However, this device did not lase in CW regime at 5 °C because the 1 μm DVS-BCB gap between silicon waveguide and microheaters introduces optical coupling between them, resulting in a higher loss of the laser cavity. When the Vernier laser shown in Fig. 13 is tuned by heating one of the MRRs, the tuning resolution is limited by the FSR of the unheated MRR. However, TDLAS of gases with narrow absorption lines requires laser sources that can be continuously tuned near the absorption lines. In order to precisely move the lasing wavelength close to gas absorption lines, both MRRs should be simultaneously heated to achieve a fine wavelength tuning [37]. Based on this method, a quasi-continuously wide tuning range of tens of nm can be realized. However, the tuning resolution is still limited by the longitudinal mode spacing of the Fabry-Perot cavity. Then we continuously tune the lasing wavelength near the absorption lines by adjusting the bias current of the gain section. The increase of bias current results in a temperature increase in the device, which leads to an increase in the refractive index of III-V waveguide and effective laser cavity length. In this method, a continuous tuning range equal to the longitudinal mode spacing of the Fabry-Perot cavity can be achieved. Fig. 16(a) show the spectral map of the fiber-coupled emission spectrum of a III-V-on-silicon Vernier laser as a function of the bias current at 5 °C. A continuous tuning range around 0.3 nm is achieved by increasing the bias current by 30 mA. The laser keeps lasing in the 0.3 nm spectral range centered at 2337.4 nm wavelength as seen in Fig. 16 (a) since the FSR of the longitudinal modes is around 0.3 nm. When the lasing mode is tuned too far from the overlapping resonant peak of the two MRRs, the laser will hop to another longitudinal mode closer to the transmission peak of the Vernier filter.

We carried out a direct absorption spectroscopy measurement of CO to verify the performance of the III-on-silicon Vernier lasers in TDLAS. Fig. 17(a) shows the HITRAN absorption spectrum of CO in the 2315 nm to 2345 nm wavelength range. Many discrete absorption lines with spacing around 2 nm can be

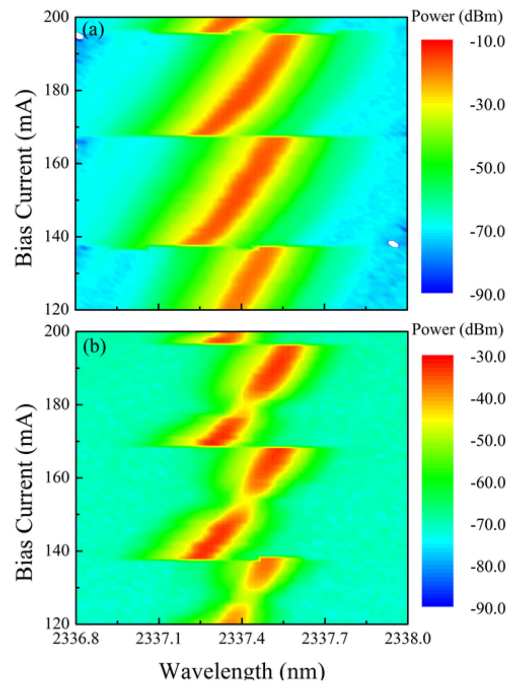


Fig. 16. (a) Contour map of the fiber-coupled emission spectra of a III-V-on-silicon Vernier laser as a function of the bias current; (b) spectral map after the light has passed through the CO gas cell.

seen. The strongest absorption is located around 2332 nm wavelength. In the TDLAS measurements, a CO gas cell identical to the one introduced in the last section was used. A III-V-on-silicon Vernier laser operated at 5 °C in CW regime is used as the laser source. In the measurements, the emission wavelength of the laser is tuned close to one of three absorption lines with different line intensity by heating both MRRs as shown in Fig. 17(b). Then high-resolution spectroscopy is achieved by continuously tuning the laser bias current. Fig. 16(b) shows a contour map of the fiber-coupled laser spectra centered at 2337.4 nm wavelength after passing through the CO gas cell. Absorption dips can be seen in the spectral map as the bias current increases from 120 mA to 200 mA. Based on the current-wavelength relationship, the TDLAS spectra and corresponding HITRAN spectra centered at 2341.2 nm are shown in Fig. 17(c). The measured absorption dip and 3 dB bandwidth match very well to the reference HITRAN data in all of three absorption lines. This result indicates the III-V-on-silicon Vernier laser is suitable for high-resolution TDLAS measurements.

V. GaSb/SILICON HYBRID EXTERNAL CAVITY LASERS

In the 2-3 μm wavelength range, semiconductor lasers implemented in GaSb-based material systems show better performance than those based on InP-based materials [23]. However, the heterogeneous integration processes of GaSb-based materials are less mature than that of InP-based devices, which results in a lower process yield and laser performance for the former [24]. Here we summarize our recent work on GaSb/silicon external cavity lasers by butt coupling a GaSb-based gain chip with a silicon photonic IC [38]. In this method, a compact widely

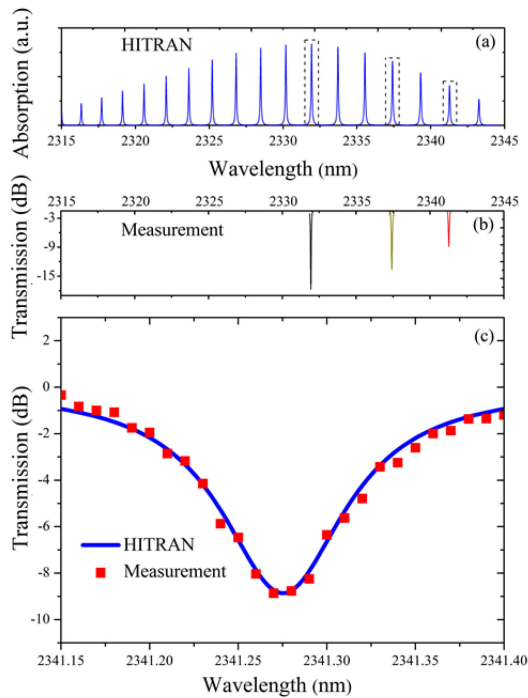


Fig. 17. (a) HITRAN absorption spectrum of CO in the 2315–2345 nm range. (b) The measured absorption spectra of three CO absorption lines. (c) Zoom-in on the measured absorption line at 2341.2 nm and the corresponding HITRAN spectrum.

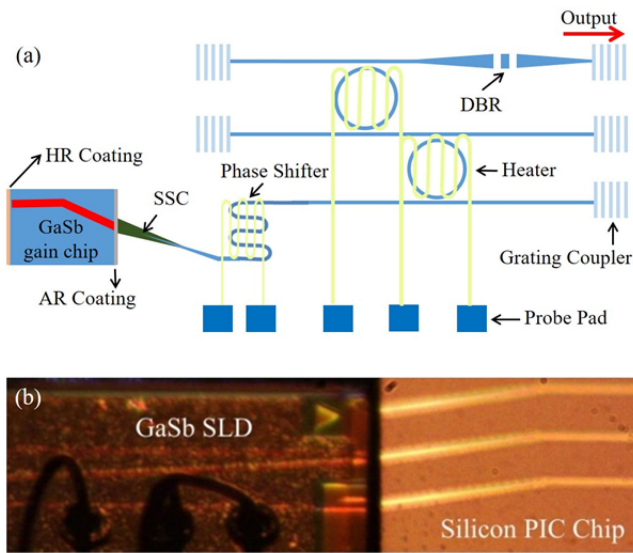


Fig. 18. (a) Schematic of the GaSb/silicon external cavity laser. (b) Top-view microscope image of the butt-coupling interface.

tunable external cavity laser can be realized by utilizing an ultra-compact silicon photonic IC and high-performance silicon photonic filters, while heterogeneous integration processes are avoided. Fig. 18(a) shows the schematic of the GaSb/silicon external cavity laser. A GaSb-based superluminescent diode (SLD) is used as the gain chip. In the 2 mm long gain chip, a HR coating with $>95\%$ reflectivity is applied on one facet while an AR coating with $<0.1\%$ reflectivity is applied on the facet close to

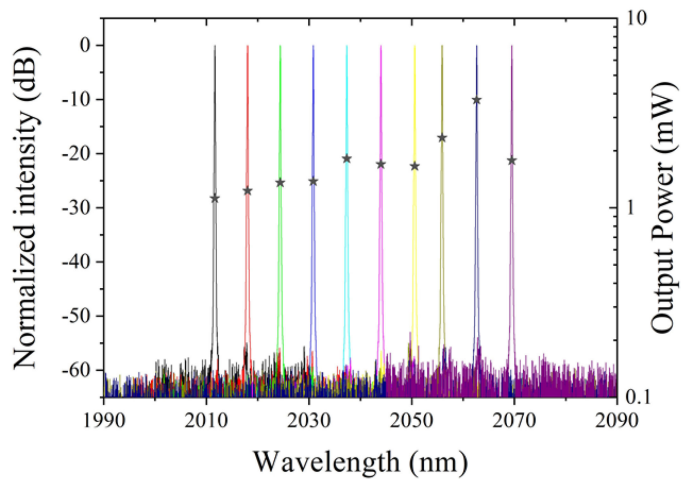


Fig. 19. Superimposed spectra and output power of the GaSb/silicon external cavity laser when the gain chip is operated uncooled.

the silicon photonic IC. The AR coated facet has a tilt-angle of 5.2 degrees to avoid self-lasing in the gain chip. The light coupling between the gain chip and silicon photonic IC is realized by a silicon SSC. To match the optical mode of the light from the gain chip, a $6 \mu\text{m} \times 0.06 \mu\text{m}$ silicon slab waveguide tilted 12 degrees is used as the facet of the silicon SSC. In order to efficiently convert the mode from the slab waveguide to that of the single mode strip waveguide ($0.7 \mu\text{m} \times 0.22 \mu\text{m}$), a 200 μm long silicon waveguide tapered from 180 nm to 700 nm is used in the SSC. Simulations indicate that the coupling loss between the gain chip and silicon slab waveguide is around 1 dB, and the mode conversion loss between the silicon slab waveguide and strip waveguide is also around 1 dB. A microscope image of the interface between the gain chip and silicon photonic IC is shown in Fig. 18(b). A Fabry-Perot laser cavity is formed between the HR-coated facet of the gain chip and the silicon DBR. In the silicon photonic IC, similar to the heterogeneously integrated laser shown in Fig. 13, a Vernier filter consisting of two silicon MRRs is used to select the lasing wavelength. In order to continuously tune the lasing wavelength without changing the bias current of the gain chip, a silicon spiral waveguide is integrated in the laser cavity as a phase shifter.

The wavelength tuning of the GaSb/silicon external cavity laser is also realized by adjusting the electrical power dissipated in the microheaters on the MRRs. Fig. 19 shows the superimposed lasing spectra of a GaSb/silicon hybrid laser operating near $2.05 \mu\text{m}$ wavelength by tuning one MRR. The GaSb-based gain chip is not cooled during measurements. A wavelength tuning range of 58 nm is achieved with a heater power consumption of 132 mW. Every ~ 12 mW electrical power change results in 6.5 nm wavelength shift. Over the full tuning range, a SMSR better than 52 dB is achieved. Similar to the heterogeneously integrated Vernier laser, a fine wavelength tuning can be achieved by simultaneously heating both MRRs and a continuous wavelength tuning can be realized by heating the phase section [38]. Under uncooled conditions, the maximum output power of the laser is around 3.8 mW and the threshold current density is

1 kA/cm². The Q-factor the MRRs used in this Vernier laser is 13500. When the Q-factor of the MRRs reduces, the output power will increase and the threshold current can reduce. For example, when the Q-factor of the MRR reduces to 2500, the uncooled laser has a maximum output power of 7.5 mW and a threshold current density of 0.8 kA/cm². However, the SMSR over the full wavelength tuning range reduces to 36 dB and the wavelength stability during tuning also decreases.

VI. CONCLUSION AND PERSPECTIVE

Integrating III–V materials or pre-fabricated gain chips with silicon photonic ICs is very promising approach to realize widely tunable laser sources for advanced spectroscopic applications. The silicon photonics platform can provide plenty high-performance building blocks for III–V/silicon lasers, such as low-loss beam combiners, widely tunable filters and ultra-compact cavities. Based on these silicon photonic components, widely tunable DFB laser arrays, Vernier lasers and external cavity lasers operating in the 2–2.5 μm wavelength range have been demonstrated. These lasers are suitable for TDLAS measurement of gases in a broad spectral range. Moreover, these III–V/silicon lasers can be integrated with silicon waveguide-based probe components and III–V/silicon photodetectors to realize fully integrated on-chip spectroscopic sensors. Further improvements on the III–V/silicon laser performance are still to be made in order to achieve better performance for practical applications. For example, the output power of the heterogeneously integrated lasers at room temperature and above should be improved. This goal can be realized by optimizing the design of the III–V epitaxial layer stack and introducing better heat spreading structures. For the III-V-on-silicon Vernier laser, the DVS-BCB passivation layer can be replaced by material with higher thermal conductivity (e.g., SiN_x) to achieve a wider tuning range in CW mode. For the GaSb/silicon hybrid laser, the Vernier filter (FSR = 65 nm) used in the current device can be replaced by a filter with larger FSR to achieve much wider tuning range. Besides, the GaSb/silicon external cavity laser configuration can be used to realize laser sources in the whole 2–2.5 μm and even at longer wavelengths considering the availability of the GaSb-based gain chips.

ACKNOWLEDGMENT

The authors would like to thank S. Verstuyft and M. Muneeb for metallization processing help.

REFERENCES

- [1] Y. A. Vlasov, "Silicon CMOS-integrated nano-photonics for computer and data communications beyond 100G," *IEEE Commun. Mag.*, vol. 50, no. 2, pp. s67–s72, Feb. 2012.
- [2] A. Spott *et al.*, "Heterogeneous integration for mid-infrared silicon photonics," *IEEE J. Sel. Topics Quantum Electron.*, vol. 23, no. 6, Nov./Dec. 2017, Art. no. 8200810.
- [3] Z. Wang *et al.*, "Novel light source integration approaches for silicon photonics," *Laser Photon. Rev.*, vol. 11, no. 4, 2017, Art. no. 1700063.
- [4] S. Chen *et al.*, "Electrically pumped continuous-wave III–V quantum dot lasers on silicon," *Nature Photon.*, vol. 10, no. 5, pp. 307–311, 2016.
- [5] T. Kita, R. Tang, and H. Yamada, "Narrow spectral linewidth silicon photonic wavelength tunable laser diode for digital coherent communication system," *IEEE J. Sel. Topics Quantum Electron.*, vol. 22, no. 6, Nov./Dec. 2016, Art. no. 1500612.
- [6] S. Xiao, M. H. Khan, H. Shen, and M. Qi, "Compact silicon microring resonators with ultra-low propagation loss in the C band," *Opt. Express*, vol. 15, no. 22, pp. 14467–14475, 2007.
- [7] F. Horst *et al.*, "Cascaded Mach-Zehnder wavelength filters in silicon photonics for low loss and flat pass-band WDM (de-)multiplexing," *Opt. Express*, vol. 21, no. 10, pp. 11652–11658, 2013.
- [8] A. Li and W. Bogaerts, "Experimental demonstration of a single silicon ring resonator with an ultra wide FSR and tuning range," *Opt. Lett.*, vol. 42, no. 23, pp. 4986–4989, 2017.
- [9] Z. Wang *et al.*, "A III-V-on-Si ultra-dense comb laser," *Light, Sci. Appl.*, vol. 6, 2017, Art. no. e16260.
- [10] T. Kita, R. Tang, and H. Yamada, "Compact silicon photonic wavelength-tunable laser diode with ultra-wide wavelength tuning range," *Appl. Phys. Lett.*, vol. 106, no. 11, 2015, Art. no. 111104.
- [11] L. Tombez *et al.*, "Methane absorption spectroscopy on a silicon photonic chip," *Optica*, vol. 4, no. 11, pp. 1322–1325, Nov. 2017.
- [12] E. M. P. Ryckeboer *et al.*, "Measurement of small molecule diffusion with an optofluidic silicon chip," *Lab Chip*, vol. 13, no. 22, pp. 4392–4399, 2013.
- [13] J. T. Robinson, L. Chen, and M. Lipson, "On-chip gas detection in silicon optical microcavities," *Opt. Express*, vol. 16, no. 6, pp. 4296–4301, 2008.
- [14] F. Dell'Olio and V. M. Passaro, "Optical sensing by optimized silicon slot waveguides," *Opt. Express*, vol. 15, no. 8, pp. 4977–4993, 2007.
- [15] M. Lee and P. M. Fauchet, "Two-dimensional silicon photonic crystal based biosensing platform for protein detection," *Opt. Express*, vol. 15, no. 8, pp. 4530–4535, 2007.
- [16] L. S. Rothman *et al.*, "The HITRAN2012 molecular spectroscopic database," *J. Quant. Spectrosc. Radiat. Transf.*, vol. 130, pp. 4–50, 2013.
- [17] S. Forouhar *et al.*, "High-power laterally coupled distributed-feedback GaSb-based diode lasers at 2 μm wavelength," *Appl. Phys. Lett.*, vol. 100, no. 3, 2012, Art. no. 031107.
- [18] D. Sanchez, L. Cerutti, and E. Tourmié, "Single-mode monolithic GaSb vertical-cavity surface-emitting laser," *Opt. Express*, vol. 20, no. 14, pp. 15540–15546, 2012.
- [19] F. Xu *et al.*, "2004-nm ridge-waveguide distributed feedback lasers with InGaAs multi-quantum wells," *IEEE Photon. Technol. Lett.*, vol. 28, no. 20, pp. 2257–2260, Oct. 2016.
- [20] S. Sprengel *et al.*, "Continuous wave vertical cavity surface emitting lasers at 2.5 μm with InP-based type-II quantum wells," *Appl. Phys. Lett.*, vol. 106, no. 15, 2015, Art. no. 151102.
- [21] N. V. Alexeeva and M. A. Arnold, "Near-infrared microspectroscopic analysis of rat skin tissue heterogeneity in relation to noninvasive glucose sensing," *J. Diabetes Sci. Technol.*, vol. 3, no. 2, pp. 219–232, 2009.
- [22] K. Vizbaras *et al.*, "High power continuous-wave GaSb-based superluminescent diodes as gain chips for widely tunable laser spectroscopy in the 1.95–2.45 μm wavelength range," *Appl. Phys. Lett.*, vol. 107, no. 1, 2015, Art. no. 011103.
- [23] A. Bauer *et al.*, "Mid-infrared semiconductor heterostructure lasers for gas sensing applications," *Semicond. Sci. Technol.*, vol. 26, no. 1, 2011, Art. no. 014032.
- [24] G. Roelkens *et al.*, "Silicon-based photonic integration beyond the telecommunication wavelength range," *IEEE J. Sel. Topics Quantum Electron.*, vol. 20, no. 4, 2014, Art. no. 8201511.
- [25] A. Spott *et al.*, "Heterogeneously integrated 2.0 μm CW hybrid silicon lasers at room temperature," *Opt. Lett.*, vol. 40, no. 7, pp. 1480–1483, 2015.
- [26] G. Boehm *et al.*, "Growth of InAs-containing quantum wells for InP-based VCSELs emitting at 2.3 μm ," *J. Cryst. Growth*, vol. 301, pp. 941–944, 2007.
- [27] S. Sprengel *et al.*, "InP-based type-II quantum-well lasers and LEDs," *IEEE J. Sel. Topics Quantum Electron.*, vol. 19, no. 4, Jul./Aug. 2013, Art. no. 1900909.
- [28] R. Wang *et al.*, "2.3 μm range InP-based type-II quantum well Fabry-Perot lasers heterogeneously integrated on a silicon photonic integrated circuit," *Opt. Express*, vol. 24, no. 18, pp. 21081–21089, 2016.
- [29] A. Gassenq *et al.*, "Study of evanescently-coupled and grating-assisted GaInAsSb photodiodes integrated on a silicon photonic chip," *Opt. Express*, vol. 20, no. 11, pp. 11665–11672, 2012.
- [30] R. Wang *et al.*, "III-V-on-silicon 2- μm -wavelength-range wavelength demultiplexers with heterogeneously integrated InP-based type-II photodetectors," *Opt. Express*, vol. 24, no. 8, pp. 8480–8490, 2016.

- [31] S. Sprengel *et al.*, "InP-based type-II heterostructure lasers for 2.5 μm working CW at room temperature and above," in *Proc. IEEE Int. Semicond. Laser Conf.*, 2014, Paper MC.05.
- [32] R. Wang *et al.*, "Heterogeneously integrated III-V-on-silicon 2.3 μm distributed feedback lasers based on a type-II active region," *Appl. Phys. Lett.*, vol. 109, 2016, Art. no. 221111.
- [33] R. Wang *et al.*, "Broad wavelength coverage 2.3 μm III-V-on-silicon DFB laser array," *Optica*, vol. 4, no. 8, pp. 972–975, 2017.
- [34] L. Bizet *et al.*, "Multi-gas sensing with quantum cascade laser array in the mid-infrared region," *Appl. Phys. B*, vol. 123, 2017, Art. no. 145.
- [35] H. Ishii *et al.*, "Widely wavelength-tunable DFB laser array integrated with funnel combiner," *IEEE J. Sel. Topics Quantum Electron.*, vol. 13, no. 5, pp. 1089–1094, Sep./Oct. 2007.
- [36] S. Pathak, M. Vanslebrouck, P. Dumon, D. Van Thourhout, and W. Boogaerts, "Optimized silicon AWG with flattened spectral response using an MMI aperture," *J. Lightw. Technol.*, vol. 31, no. 1, pp. 87–93, Jan. 2013.
- [37] R. Wang *et al.*, "Widely tunable 2.3 μm III-V-on-silicon Vernier lasers for broadband spectroscopic sensing," *Photon. Res.*, vol. 6, no. 9, pp. 858–866, 2018.
- [38] R. Wang *et al.*, "Compact GaSb/silicon-on-insulator 2.0 \times μm widely tunable external cavity lasers," *Opt. Express*, vol. 24, no. 25, pp. 28977–28986, 2016.

Ruijun Wang received the B.S. degree in material science and engineering from Xidian University, Xi'an, China, the M.S. degree in material physics and chemistry from Shandong University, Jinan, China, and the Ph.D. degree in photonics engineering from Ghent University, Ghent, Belgium. He is currently a Postdoctoral Researcher with Institute for Quantum Electronics, ETH Zurich, Zurich, Switzerland. Prior to joining the ETH Zurich, he was a Postdoctoral Researcher with Photonics Research Group of Ghent University-IMEC from 2017 to 2018. His current research interests include semiconductor lasers, photonic integrated circuits, frequency comb, infrared spectroscopy, and high-speed photodetectors.

Bahawal Haq received the B.S. degree in engineering sciences from the Ghulam Ishaq Khan Institute of Engineering Sciences and Technology, Pakhtunkhwa, Pakistan, in 2013, the M.S. degree in microsystems engineering from Masdar Institute, Abu Dhabi, UAE, in 2016. He is currently working toward the Ph.D. degree at Photonics Research Group, Ghent University, Ghent, Belgium. His current research interests include heterogeneous integration of III-V/Si for the development of lasers and SOAs.

Stephan Sprengel was born in Erding, Germany, in 1987. He received the Dipl.Phys. degree from Technische Universität München, München, Germany, in 2012. Since then he has been working toward the Ph.D. degree with the Walter Schottky Institut, Technische Universität München. He is currently involved in the research on InP and GaSb-based type-I and type-II quantum well lasers, LEDs, and photodiodes for the mid-infrared including design, epitaxial growth, manufacturing, and characterization. He is a member of the Deutsche Physikalische Gesellschaft and the IEEE Photonics Society.

Aditya Malik received the bachelor's degree in physics from Delhi University, the M.Sc. degree in physics from IIT Delhi, and the Ph.D. degree from the Photonics Research Group, Ghent University, Ghent, Belgium, in March 2015, developing a novel CMOS compatible waveguide platform beyond the telecommunication wavelength range. He was a DAAD Fellow in FU Berlin during his master studies. After receiving the Ph.D. degree, he worked on various topics such as realizing integrated gas sensors, external cavity tunable lasers, and wavelength demultiplexers operating in mid-infrared. His current research interest is integration of mid-infrared light sources on CMOS compatible passive waveguide platforms. He has authored or coauthored more than 35 journal and conference papers which have been cited more than 700 times.

Anton Vasiliev received the B.Sc. degree in applied physics engineering in 2012 and the M.Sc. degree in photonics in 2014 from Ghent University, Ghent, Belgium. He is currently working toward the Ph.D. degree in photonics with the Photonics Research Group, Department of Information Technology, IMEC, Ghent University, Ghent, Belgium. His current research interests include integrated circuits on SOI platform for mid-infrared spectroscopy applications and photothermal methods for trace gas detection. He is a member of the IEEE Photonics Society and the OSA Optical Society.

Gerhard Boehm was born in Munich, Germany, in 1962. He received the Dipl.Ing. degree in technical physics from Fachhochschule Muenchen, Munich, Germany, in 1988. Since then he has been with the Walter Schottky Institut, Technical University of Munich, Munich, Germany. His main interests include epitaxial growth of III-V semiconductor structures, quantum cascade lasers, and long-wavelength vertical-cavity and edge-emitting laser diodes.

Ieva Šimonytė received the M.Sc. degree in material science and semiconductor physics in 2014 from Vilnius University, Vilnius, Lithuania. Since 2013, she has been working as a Computational Simulation Engineer in Brolis Semiconductors, Vilnius, Lithuania. Her activities include electrical, thermal, and optical modeling of semiconductor material, devices and systems, simulations of light interaction with living body, and statistical data analysis. She has authored or coauthored more than 15 papers in scientific peer-reviewed journals and conference proceedings and six pending patent applications.

Augustinas Vizbaras received the B.S. degree in electrical engineering in 2007 from Vilnius University, Vilnius, Lithuania, the M.Sc. degree in physics in 2009 from the Royal Institute of Technology, Stockholm, Sweden, and the doctoral degree in the field of semiconductor technology in 2012 from the Walter Schottky Institut, TU Munich, Munich, Germany. In 2011, he co-founded Brolis Semiconductors, Vilnius, Lithuania, where he currently heads the chip technology and sensor activities. He has authored or coauthored more than 50 papers in scientific peer-reviewed journals and conference proceedings, three granted U.S. patents, and nine pending international patent applications. He was awarded with the Order of Merit to Lithuania Knights Cross in 2017, the Medal for Distinguished Service from Lithuanian Special Operation Forces in 2018, and the Medal for Merit to Lithuania's Riflemen's Union in 2015.

Kristijonas Vizbaras received the B.S. degree in electrical engineering in 2007 from Vilnius University, Vilnius, Lithuania, the M.Sc. degree in physics in 2009 from the Royal Institute of Technology, Stockholm, Sweden, and the Doctoral degree in the field of semiconductor technology in 2012 from the Walter Schottky Institut, TU Munich, Munich, Germany. In 2011, he co-founded Brolis Semiconductors, Vilnius, Lithuania, where he currently heads the epitaxial growth activities. He has authored or coauthored more than 50 papers in scientific peer-reviewed journals and conference proceedings, two granted U.S. patents, and nine pending patent applications. He was awarded with the Order of Merit to Lithuania Knights Cross in 2017, the Medal for Distinguished Service from Lithuanian Special Operation Forces in 2018, and the Medal for Merit to Lithuania's Riflemen's Union in 2015.

Joris Van Campenhout received the master's degree in physics engineering in 2002 and the Ph.D. degree in electrical engineering in 2007, both from Ghent University, Ghent, Belgium. After receiving the Ph.D. degree, he was a Postdoctoral Researcher with the IBM T. J. Watson Research Center, New York, NY, USA. In 2010, he joined IMEC, Belgium, where he is currently the Program Manager Optical I/O.

Roel Baets received the M.Sc. degree in electrical engineering from Ghent University (UGent), Ghent, Belgium, in 1980, the second M.Sc. degree from Stanford University, Stanford, CA, USA, in 1981, and the Ph.D. degree from UGent, in 1984. He is a Full Professor with UGent and is associated with IMEC. From 1984 to 1989, he held a postdoctoral position with IMEC. Since 1989, he has been a Professor with the Faculty of Engineering and Architecture, UGent, where he founded the Photonics Research Group. From 1990 to 1994, he was a part-time Professor with Delft University of Technology and from 2004 to 2008 with Eindhoven University of Technology. He has mainly worked in the field of integrated photonics. As part of a team of eight professors, he leads the Photonics Research Group. In 2006, he founded the ePIXfab, the globally first multiproject-wafer service for silicon photonics. Since then ePIXfab has evolved to become the European Silicon Photonics Alliance. He is also the Director of the multidisciplinary Center for Nano- and Biophotonics with UGent, founded in 2010. He was a co-founder of the European M.Sc. programme in photonics. He is an ERC Grantee of the European Research Council and a Methusalem Grantee of the Flemish government. He is a Fellow of the European Optical Society and Optical Society. He is also a member of the Royal Flemish Academy of Belgium for Sciences and the Arts.

Markus-Christian Amann was born in Singen/Hohentwiel, Germany, in 1950. He received the Diploma in electrical engineering and the Dr. Ing. degree from Technische Universität München, Munich, Germany, in 1976 and 1981, respectively. From 1981 to 1994, he was with the Corporate Research Laboratories, Siemens AG, Munich, where he was involved in the research on long-wavelength InGaAsP–InP laser diodes. In 1990, he became the Deputy Director for the research on laser diodes and integrated optoelectronic devices. On February 1994, he joined as a Full Professor in “Technical Electronics” with the Department of Electrical Engineering, University of Kassel, where he established a working group for III/V semiconductor electronics and optoelectronics. Since November 1997, he has been the Chair of semiconductor technology with the Walter Schottky Institut, Technische Universität München, Garching. He has authored or coauthored about 400 articles and talks on semiconductor optoelectronics in scientific journals, conference proceedings, and coauthored two books. He is a member of the German Informationstechnische Gesellschaft and a Fellow of the IEEE Photonics Society. He was a member of numerous conference committees such as the IEEE Semiconductor Laser Conferences, the Indium Phosphide and Related Materials Conferences, and the Conferences on Lasers and Electro-Optics.

Gunther Roelkens received the degree in electrical engineering and the Ph.D. degree from the Department of Information Technology, Ghent University, Ghent, Belgium, in 2002 and 2007, respectively. He is currently a Full Professor with Ghent University. In 2008, he was a Visiting Scientist with the IBM T. J. Watson Research Center, Rochester, NY, USA. He was an Assistant Professor with Eindhoven University of Technology, Eindhoven, The Netherlands. His research interests include the heterogeneous integration of III–V semiconductors and other materials on top of silicon waveguide circuits and electronic/photonics co-integration. He was a holder of an ERC starting Grant MIRACLE to start up research in the field of integrated mid-infrared photonic integrated circuits.